Realization of High-Voltage Output on Monolithic Silicon Solar Cells in Series for Self-Powered Systems

Taojian Wu, Hao Lin,* Liyan Chen, Zhaolang Liu, Yicong Pang, Zhengping Li, Pingqi Gao,* and Wenzhong Shen*

Crystalline silicon solar cells dominate the photovoltaic market nowadays. However, they are rarely used in self-powered systems (with an operating voltage of 1.5~12.0 V) mainly because of the low integration of silicon solar cell modules, which need slicing and then series connection. Herein, a series-interconnected solar cell which can be prepared on a monolithic silicon wafer, with the capability to output high voltage by controlling the number of sub-cells, is proposed. Further, based on a technology computer aided design (TCAD) numerical simulation, an in-depth analysis of an unconventional non-shunt resistance type of leakage mechanism under electric and light injection which has not been reported before is proposed and performed, finding that the leakage current can be divided into three stages that are closely related to the variation in the conductivity (resistance) of the transition region (TR) under injection conditions. Then, several targeted methods especially an unusual method of increasing the recombination to constrain the rise in conductivity in TR are proposed to improve its efficiency by suppressing leakage current at different stages. Finally, simulation reveals that the proposed monolithic on-chip solar micromodules enable not only high voltage but also high efficiency (≥24.0%), which well meets the requirements of self-powered systems at low cost.

1. Introduction

Self-powered devices are of increasing interest due to their multifunctional performance and environmental friendliness. Light, motion/vibration, thermal gradients, and radio frequency (RF) electromagnetic radioactivity comprise the main energy sources from the ambient for self-powered systems.[1] Motion/vibration and thermal gradients energy are widely available but with low-power density, and the devices harnessing them are compact and convenient, which are generally used in wearable electronic devices. Additionally, the devices that exploit thermal gradient energy are accompanied with a low energy-conversion efficiency.[1–6] As for the devices that collect RF energy, they have to deal with very low-power density levels.[7,8] In contrast, solar energy is endowed with universality, inexhaustibility, and high-power density.[9] With the continuous improvement of photoelectric conversion efficiency, solar energy accounts for an increasing share of the energy supply system, gradually becoming one of the main alternatives to fossil energy.[10]

For most electronics, the operating voltage is generally 1.5~12.0 V (i.e., a few dry batteries or button batteries). For example, the silicon impact ionization metal–oxide–semiconductor (I-MOS) field-effect transistors require a supply voltage of ~5.5 V.[11,12] Concerning the conventional single junction solar cells, the open-circuit voltage (V_{OC}) depends on the bandgap of the semiconductor material and the intensity of sunlight.[13] Taking silicon solar cell as an example, the V_{OC} is generally less than 0.75 V under a standard air mass (AM) 1.5G spectrum (1000 W m^{-2}). As a result, the high-voltage requirement is difficult to be met by single junction solar cells alone. Thin-film solar cell modules, such as CuInGaSe solar cell

T. Wu, L. Chen, Z. Li, W. Shen
Institute of Solar Energy
Key Laboratory of Artificial Structures and Quantum Control (Ministry of Education)
School of Physics and Astronomy
Shanghai Jiao Tong University
800 Dong Chuan Road, Shanghai 200240, China
E-mail: wzshen@sjtu.edu.cn

H. Lin, Z. Liu, Y. Pang, P. Gao
School of Materials
Sun Yat-sen University
Guangzhou 510275, China
E-mail: linh229@mail.sysu.edu.cn; gaopq3@mail.sysu.edu.cn

H. Lin, P. Gao
Institute for Solar Energy Systems
Guangdong Provincial Key Laboratory of Photovoltaic Technology
State Key Laboratory of Optoelectronic Materials and Technologies
Sun Yat-sen University
Guangzhou 510275, China

P. Gao
Jiangsu Collaborative Innovation Center of Photovoltaic Science and Engineering
Changzhou University
Changzhou 213164, China

modules, can achieve high-voltage output by interconnecting multiple CuInGaSe solar cells in series on a single substrate.[14] Monolithic tandem solar cells stacking solar cell materials with different bandgaps are also capable of high-voltage output.[15] For instance, a GaInP/GaAs/Ge triple junction solar cell with a V_{OC} of 2.5 V was integrated vertically with a Au/ZnO Schottky diode by Hou et al., achieving a self-biased ZnO-based humidity sensor.[16] Both of thin-film solar cell modules and monolithic tandem solar cells are suitable to integrate with electronics to realize a self-powered system. Nevertheless, now they are suffering from high cost, low conversion efficiency, instability or difficulty in large-scale production, etc., compared to crystalline silicon solar cells.[15–19]

Actually, crystalline silicon solar cell is the most mature and widely used type of solar cells with a market share of over 90% nowadays.[20,21] However, it is rarely used in self-powered systems mainly because of the low integration of silicon solar cell modules with the capability of high-voltage output, which need slicing and then series connection. Here, we propose a

series-interconnected solar cell that can be prepared on a monolithic silicon wafer, we call it series-interconnected monolithic silicon (SCMS) solar cell, its structure is shown in **Figure 1**a, b. The output voltage can be controlled by the number of sub-cells connected in series, achieving adjustable and high-voltage output. Moreover, more than 90% of all the semiconductor products are made of silicon,[22] and it is promising and of great significance to integrate silicon solar cells with silicon-based chips to achieve self-powered chips.

It should be noted that there is almost no reports on SCMS solar cells except that Nordmann et al. have proposed a similar structure, but with part of the silicon removed to form deep groove isolation to reduce leakage current.[23,24] However, its complex fabrication process and low efficiency (≤18.7%) reduce the application potential. Therefore, without complicated grooving or traditional slicing methods, how high-efficiency SCMS solar cells can be obtained becomes the main research object in this study. Our analysis found that leakage channel in SCMS solar cells is the main difference between SCMS solar
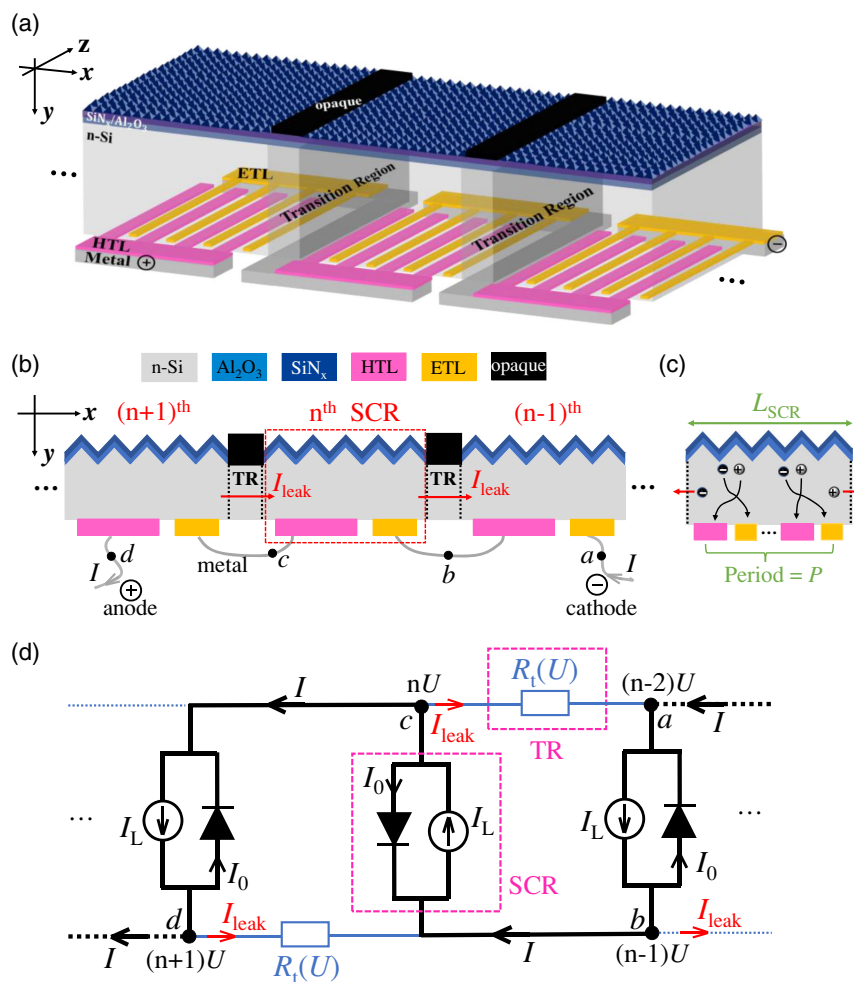
Figure 1. a) The 3D sketch and b) cross section of the series-interconnected monolithic silicon (SCMS) solar cells. c) Specific structure of one sub-cell region (SCR). L_{SCR} is the width of the SCR. d) Simplified equivalent circuit of the SCMS solar cells. The black bold line represents the main current channel, the direction of I is the direction of the total current under illumination (i.e., a–b–c–d). The blue line represents the leakage channel, I_{leak} is the leakage current flowing through each transition region (TR). Note that since the TRs are inherently a semiconductor, the resistance of R_t varies under electric and light injection, the role of TRs is not simply a shunt resistance known from the equivalent circuit model of a solar cell.[27]

cells and normal interdigitated back contact (IBC) solar cells.[25,26] Here, through a silvaco TCAD-based numerical simulation, we not only clearly demonstrated the properties of leakage current during electric injection and light injection, but also proposed and performed an in-depth analysis of an unconventional non-shunt resistance type of leakage mechanism under electric and light injection, which has not been reported before, supported by current density map, band diagram, and mathematical equation fitting of the leakage current. Based on our deep understanding of the leakage mechanism, several practical methods including an unusual method of increasing the recombination to constrain the rise in conductivity in the transition region (TR) have been proposed to improve the performance of the SCMS solar cells by suppressing leakage current, and the simulation results showed that an V_{OC} of $(0.767 \times N)$ V (N is the number of sub-cells) and an η of more than 24.0% of the SCMS solar cells (the thickness of silicon wafer is 62 μm) can be realized for homojunction. This means the SCMS solar cells can not only achieve high-voltage output by controlling the number of sub-cells, but also maintain high efficiency level, which well meets the requirements of self-powered systems at low cost.

2. Structure and Simplified Equivalent Circuit of SCMS Solar Cells

Figure 1a,b shows the 3D sketch and the cross section of the SCMS solar cells, respectively. The differences between SCMS and normal IBC solar cells can be observed as follows: one is that there are equally spaced opaque objects on top of the n-Si bulk of the SCMS solar cells for shading and we call the silicon regions directly below the opaque objects the TRs, which divide the whole SCMS solar cell into several identical sub-cell regions (SCRs), thus an SCMS solar cell consists of n SCRs and $(n - 1)$ TRs (n is an integer), as shown in Figure 1b. The other refers to the position of the electrodes, the anode and cathode of the middle SCR are connected in series with the cathode of the previous SCR and the anode of the next SCR, respectively. As we can observe in Figure 1a, between adjacent SCRs, hole-transport layers (HTLs) and electron-transport layers (ETLs) are in series, while inside each SCR, all the HTLs are connected in parallel and same for all the ETLs. In addition, parts of the electrodes are deposited under the TRs to achieve this series connection. To isolate electrodes from the TRs, only insulating layers (not shown in the figure) need to be inserted between electrodes and TRs, which can easily fabricate through physical mask. Only one pair of HTL/ETL inside each SCR is shown for simplicity in Figure 1b, in fact each SCR contains multiple pairs of HTL/ETL as shown in Figure 1c. If there are P pairs of HTL/ETL inside each SCR, we define the Period of SCMS solar cells is P and L_{SCR} is the width of each SCR. Since the width of HTLs, ETLs, and their gaps are fixed, a larger value of Period means a larger L_{SCR}. The aforementioned monolithic silicon solar cell fabricated by Nordmann et al.[23,24] actually reduces leakage current by digging a deep groove in the TRs, but as a consequence, it significantly increases the complexity of the process. If the resistivity of each TR of our SCMS solar cells is infinite, the TRs are similarly removed, they can completely isolate the SCRs.

Concerning the direction of carrier transport in the SCMS solar cells, similar to normal IBC solar cells, holes move to the HTLs and electrons move to the ETLs under illumination inside the SCRs as demonstrated by the black arrows in Figure 1c. In addition, some holes and electrons flow through the TRs causing leakage current as revealed by the red arrows in Figure 1b,c, which do not flow through the metal wires to form effective current in circuit. Obviously, the presence of this leakage channel is the biggest difference between the SCMS solar cells and normal IBC solar cells. A simplified equivalent circuit of the SCMS solar cells is showed in Figure 1d to facilitate the understanding of the working principle of the SCMS solar cells and the difference with normal IBC solar cells. The black bold line represents the main current channel, and the direction of I in the figure is the direction of the total current under illumination (i.e., a–b–c–d). The blue line represents the leakage channel, and I_{leak} is the leakage current flowing through each TR. According to the equivalent circuit model of a basic p–n junction solar cell, under ideal conditions (i.e., ignoring series and shunt resistance), it is equal to a diode that represents the p–n junction and a current-generation component that represents the diffusion current of light-generated carriers.[27] Each SCR can then be equal to a diode and a current-generation component, I_0 is the current flowing through the diode, and I_L is the photocurrent. We can easily get

$$I = I_L - I_0 - I_{leak} \tag{1}$$

If countless SCRs are connected in series, the voltage drop of each SCR is equal because each SCR is exactly the same. Assuming the voltage drop is U, the potential at points a, b, c, and d is $(n - 2)U$, $(n - 1)U$, nU, and $(n + 1)U$, respectively. Obviously, because there exists a voltage drop on both sides of the TRs, this must cause the leakage current in TRs. It should be noted that, since the TRs are inherently a semiconductor, though we use a resistor R_t to describe the TR, actually the leakage current in the TR is extremely complex, and the resistance of R_t varies under electric and light injection. Therefore, the leakage current does not simply vary linearly with U, and the role of TRs is not simply a shunt resistance known from the equivalent circuit model of a solar cell.[27] The leakage mechanism is the core of the study in this paper. Understanding the causes of leakage current helps us to radically reduce leakage current, and to further improve the efficiency of the SCMS solar cells.

3. Mechanism of Leakage Current Under Electric Injection

To enable a more detailed observation of the characteristics of the leakage current, the curve of leakage current of the SCMS solar cell (Period = 8, L_{SCR} = 16.2 mm, and the corresponding surface area S of a sub-cell is 1.62×10^{-4} cm²) under only electric injection versus voltage is provided in **Figure 2**a. Note that the horizontal axis "voltage" in the figure represents "U" in Figure 1d, that is, the voltage drop of each SCR (the "voltage" in this paper represents 'U' unless special instructions). The simulation method and extraction method of leakage current
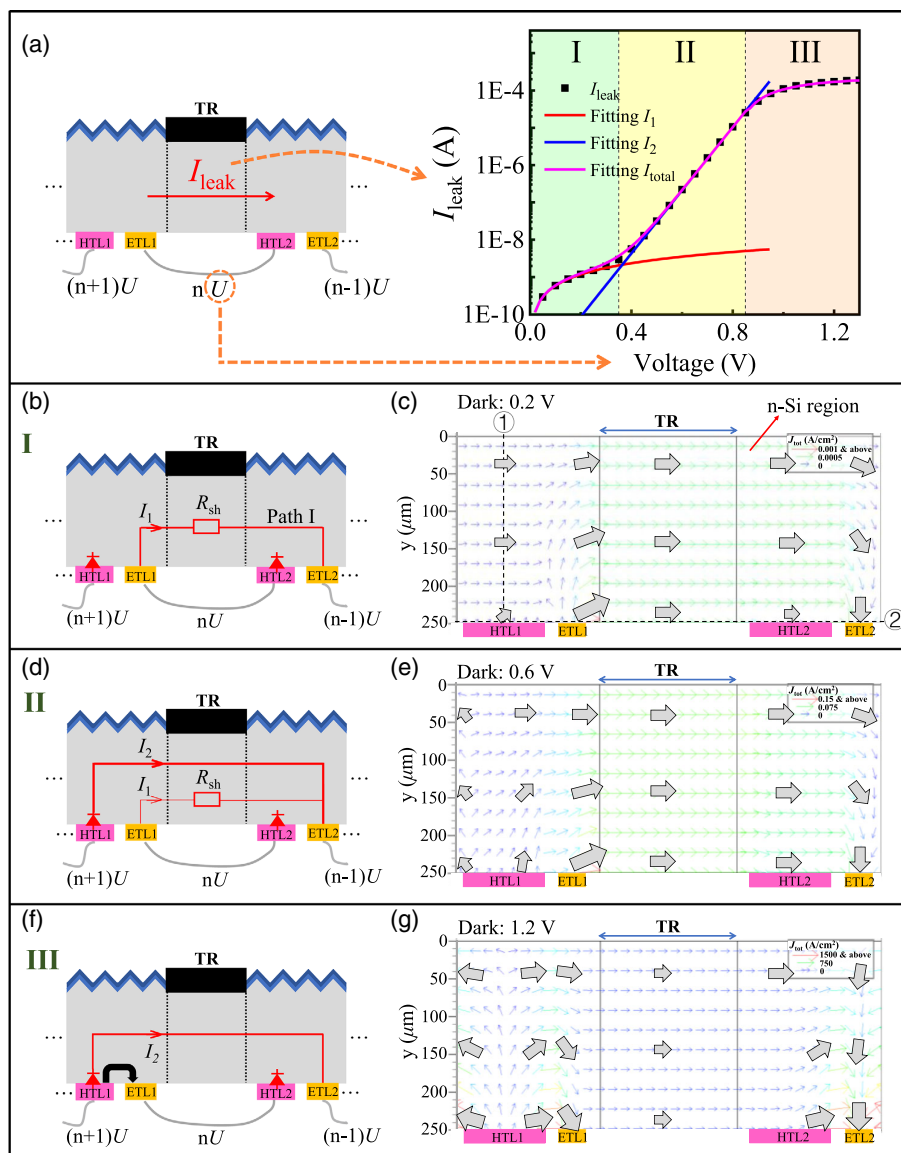
Figure 2. a) Dark $I_{leak} - U$ curve of the SCMS solar cell (Period $= 8$, $L_{SCR} = 16.2$ mm, $S = 1.62 \times 10^{-4}$ cm^2), which can be divided into three stages (linear variation, exponential variation, and saturation stage). Schematic diagram of the leakage circuit at stages b) I, d) II, and f) III, and the corresponding dark current density map by simulation when applied voltage are c) $U = 0.2$ V, e) $U = 0.6$ V, and g) $U = 1.2$ V. Where, in (a), the fitting results are $R_{sh} = 1.7 \times 10^8 \, \Omega$, $I_{02} = 1.8 \times 10^{-12}$ A, and $m = 2$.

are detailed in Methodology. The leakage current does not simply vary linearly with U as mentioned previously, but can be divided into three stages: I) linear variation stage at low voltage; II) exponential variation stage at moderate voltage; and III) saturation stage at high voltage. For convenience, we call the two pairs of HTL/ETL nearest to TR as HTL1/ETL1 and HTL2/ETL2, respectively. Simulation result shows that the leakage current exhibits an independence from Period, which indicates the leakage current only comes from the regions above HTL1/ETL1 and HTL2/ETL2 (Methodology). Therefore, we only need to focus on the region consisting of HTL1/ETL1, HTL2/ETL2, and TR (Figure 2a, left) to study the leakage mechanism.

3.1. Direction of Leakage Current at Three Stages

According to analysis of dark current density maps and band diagrams, we propose the schematic diagram of the leakage circuit at three stages, where, band diagrams are described in **Figure 3**, while the other two are showed in Figure 2. As shown in Figure 2b,c), they illustrate the schematic diagram of the leakage circuit at stage I and corresponding dark current density map by simulation when applied voltage is $U = 0.2$ V, respectively (the complete dark current density maps in these three stages are shown in Figure S2, Supporting Information). At this stage, the leakage current mainly comes from the region above ETL1 and flows to ETL2 (I_1). R_{sh} representing a shunt resistance in
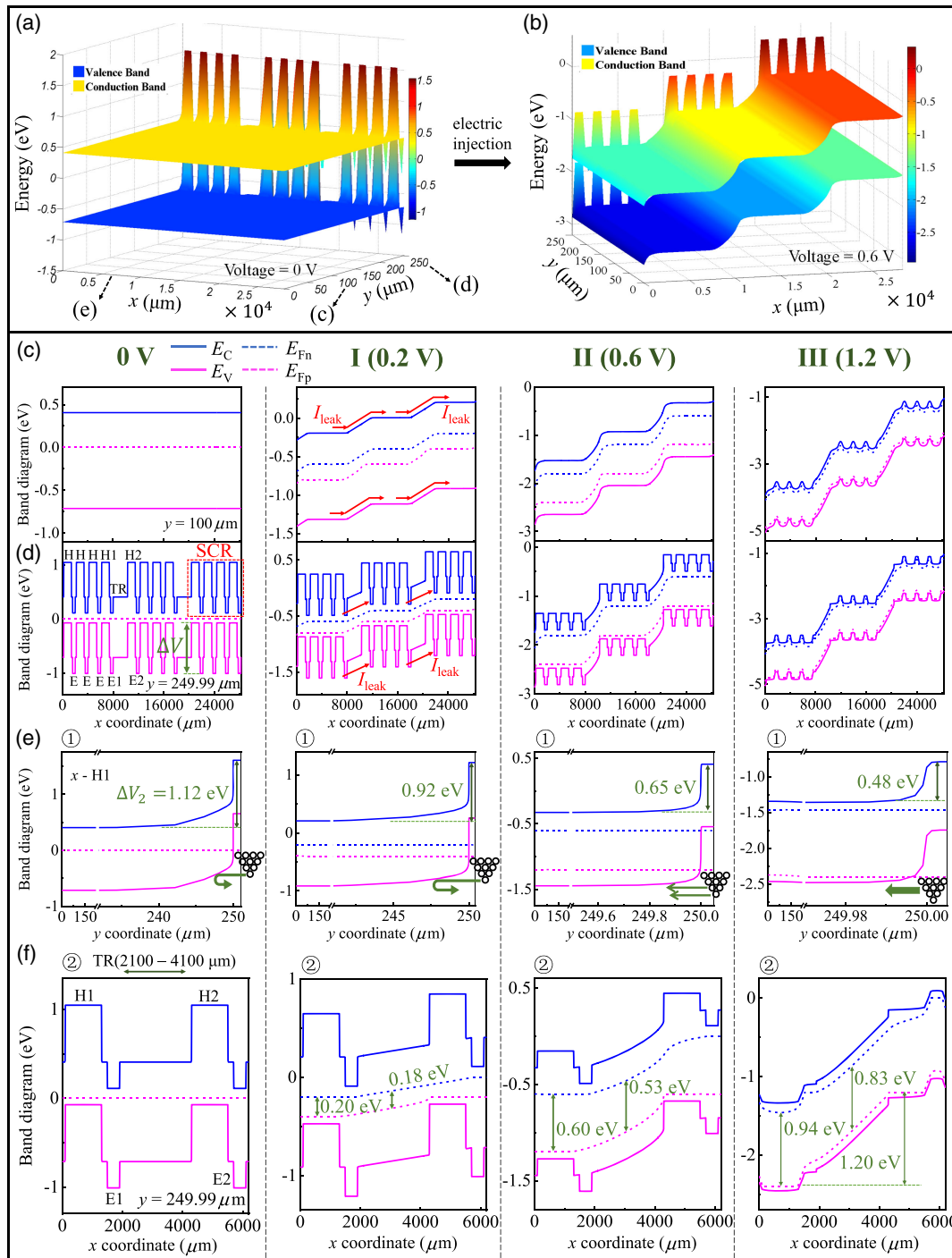
Figure 3. The 3D dark band diagram of 3 consecutive sub-cells in series in a SCMS solar cell (Period = 4) at a) $U = 0$ V and b) $U = 0.6$ V. The corresponding 2D band diagram in the x direction at c) $y = 100 \, \mu m$ and d) $y = 249.99 \, \mu m$ with different voltages (0 V state and three stages). e) The corresponding 2D band diagram in the y direction at $x = 6700 \, \mu m$ (middle of hole-transport layer [HTL]1 region) with different voltages. ①: 2D band diagram in Figure 2c with different voltages. f) A local detailed view of Figure d), consisting of HTL1/electron-transport layer [ETL]1, HTL2/ETL2, and TR. ②: 2D band diagram in Figure 2c with different voltages. "H" in these figures represents "HTL" and "E" represents "ETL".

the equivalent circuit model of a basic p–n junction solar cell[27] is used to describe the resistance of the leakage circuit. It is well known that, in the contact region between HTLs and n-Si region,

it will form large band upward bending, acting like a diode. In contrast, it forms ohmic contact between ETLs and n-Si region due to low band bending and major carrier transmission, leading

to I_1 dominate at low voltage. Figure 2d,e shows the situation of stage II. At this stage, the leakage current I_2 dominates, which comes from the region above HTL1 and flows to ETL2. Concerning stage III, most current flows from the HTLs to the closest ETLs inside the same SCR, only a small part of the current flows to the TRs as shown in Figure 2f,g. The I_2 is still dominant, but gradually saturates.

Based on the previous analysis, the following formula is applied to fit the stages I and II of the $I_{leak} - U$ curve in Figure 2a

$$I_{leak} = I_1 + I_2 = \frac{U}{R_{sh}} + I_{02}\left[\exp\left(\frac{U}{mV_T}\right) - 1\right], U \leq 0.85\,V \quad (2)$$

A good agreement can be observed. $I_1 = \frac{U}{R_{sh}}$ is the linear leakage current at stage I, and $I_2 = I_{02}[\exp\left(\frac{U}{mV_T}\right) - 1]$ is the exponential leakage current at stage II. The fitting results are $R_{sh} = 1.7 \times 10^8\,\Omega$, $I_{02} = 1.8 \times 10^{-12}\,A$, and $m = 2$. R_{sh} was found to be very close to the resistance of the path in the x direction of I_1 (we call it path I) as shown in Figure 2b: $R_I = \rho\frac{L_1}{t \times d} = 1000\,\Omega\,cm \times \frac{4200\,\mu m}{250\,\mu m \times 1\,\mu m} = 1.68 \times 10^8\,\Omega$, where $L_1 = 4200\,\mu m$ is the average distance between ETL1 and ETL2 in the x direction, that is, the average length of path I. ρ and t are the resistivity and thickness of silicon wafer, respectively, and d is the length of TR in the z direction (the default parameters in this simulation are detailed in Methodology), thus $t \times d$ is the cross-sectional area of the TR (path I). As for stage III, it is a saturation stage (not a linear variation stage) and we fit it with a polynomial as detailed in Figure S3, Supporting Information. The difference between the dark current–voltage ($I–V$) curve of a sub-cell and the dark $I_{leak} - U$ curve of the SCMS solar cell can also be found in Figure S3, Supporting Information.

3.2. Analysis of Band Diagrams at Three Stages

For a clear understanding of the leakage mechanism, a complete band diagram is required. As shown in Figure 3a,b), they are 3D dark band diagrams of 3 consecutive sub-cells in series in a SCMS solar cell (Period = 4) at $U = 0$ and $U = 0.6\,V$, respectively. We divide the n-Si region (with a thickness of 250 μm) into a bulk region ($\gamma \leq 245\,\mu m$) and a selective contact region ($245 < \gamma < 250\,\mu m$) near the carrier collection layer according to the γ coordinate. Figure 3c,d provides the corresponding 2D band diagram in the x direction at $\gamma = 100\,\mu m$ (bulk region) and $\gamma = 249.99\,\mu m$ (selective contact region) with different voltages (0 V state and three stages), respectively. We can observe that the quasi-Fermi levels in the TRs as well as the regions above HTL1/ETL1 and HTL2/ETL2 are flat when the applied voltage $U = 0\,V$, but are inclined at stages I, II and III, since there is a voltage drop on both sides of each TR (i.e., the voltage drop between ETL1 and ETL2 or between HTL1 and HTL2). Therefore, the carriers near the TRs flow to TRs driven by electric field, resulting in leakage. In addition, a barrier ΔV exists between the adjacent HTLs and ETLs inside the SCRs in the selective contact region, as illustrated by the green arrow in Figure 3d, causing the carriers transport in the x direction being difficult. As a result, the leakage current only comes from the

regions above HTL1/ETL1 and HTL2/ETL2. A more detailed explanation can be found in Figure S2, Supporting Information. The direction of the leakage current is shown by the red arrows in the figure, and leakage indeed exists at both the left and right edges of the SCRs.

At stage I of leakage, the I_1 dominates, which comes from the region above ETL1, since it is ohmic contact between ETLs and n-Si region while there is a large barrier ΔV_2 in the contact region between HTLs and n-Si region at this time. As shown in Figure 3e, it is the 2D band diagram in the γ direction at $x = 6700\,\mu m$ (middle of HTL1 region) with different voltages. As the voltage increases, this barrier ΔV_2 decreases from 1.12 eV at $U = 0\,V$ to 0.65 eV at $U = 0.6\,V$. Thus, more and more holes can cross the barrier, as shown by the hollow circles and green arrows, causing the I_2 to exceed I_1, and then I_2 dominates at stage II. When at a high-voltage level, ΔV disappears completely and reverses, as shown in Figure 3c,d at stage III, thereby most current flows from the HTLs to the closest ETLs inside the same SCR, only a small part of the current flows to the TRs.

3.3. Theoretical Analysis of Linear, Exponential Variation or Saturation of the Leakage Current, and the Origin of the Ideality Factor m

According to the current equation of drift and diffusion, the total electron current J_n and the total hole current J_p can be expressed as[13]

$$J_n = \frac{\sigma_n}{q}\nabla E_{Fn} \quad (3)$$

$$J_p = \frac{\sigma_p}{q}\nabla E_{Fp} \quad (4)$$

where, q is the electron charge. E_{Fn} and E_{Fp} are the quasi-Fermi levels of electrons and holes, respectively, and ∇E_F is related to electric field (namely applied voltage). σ is the corresponding conductivity of a semiconductor, which is related to the carrier concentration[13]

$$\sigma = Nq\mu = (N_0 + \Delta N)q\mu \quad (5)$$

where, N is the total carrier concentration in the semiconductor, including the carrier concentration N_0 at thermal equilibrium (i.e., related to the doping concentration) and the injected non-equilibrium carrier concentration ΔN. μ is the carrier mobility. In addition, the concentration of electron (n) and hole (p) at non-equilibrium satisfies[13]

$$np = n_i^2\exp\left(\frac{E_{Fn} - E_{Fp}}{kT}\right) \quad (6)$$

where, n_i corresponds to the intrinsic carrier concentration. k is Boltzmann's constant and T is the thermodynamic temperature. At stage I of the leakage, $\Delta N \ll N_0$, leading to $N \approx N_0$, $\sigma \approx \sigma_0$, which is the initial conductivity. Therefore, the conductivity of the regions along path I remains unchanged at stage I. The quasi-Fermi levels of the regions along path I are found to be straight at stage I in Figure 3c,d, that is, ∇E_{Fn} and ∇E_{Fp} do

not change with the x coordinate. And they both vary linearly with voltage at stage I according to the simulation results, resulting in a linear variation in the leakage current with voltage. In contrast, at stage II, $\Delta N \gg N_0$. The electron concentration is approximately equal to the hole concentration, since the injected electron and hole concentrations are equal. According to Equation (6), we can obtain

$$n \cong p \cong n_i \exp\left(\frac{E_{Fn} - E_{Fp}}{2kT}\right) \qquad (7)$$

Combining with Equation (5), we get

$$\sigma = 2n_i q\mu \exp\left(\frac{E_{Fn} - E_{Fp}}{2kT}\right) \qquad (8)$$

Disregarding recombination temporarily (SRH lifetime is long enough), the quasi-Fermi-level splitting (QFLS) is dictated by the voltage drop V in this region, it can be expressed as[13]

$$E_{Fn} - E_{Fp} = qV \qquad (9)$$

As shown in Figure 3f, it corresponds to a local detailed view of Figure 3d, consisting of HTL1/ETL1, HTL2/ETL2, and TR. The QFLS of the regions along path I are 0.20 or 0.18 eV at $U = 0.2$ V and are 0.60 or 0.53 eV at $U = 0.6$ V, that is, they are all found close to qU at stages I and II since the voltage drop on both sides of the TR is U. Thereby the conductivity here is

$$\sigma = 2n_i q\mu \exp\left(\frac{U}{2V_T}\right) = C \exp\left(\frac{U}{2V_T}\right) \qquad (10)$$

where, C is a constant and $V_T = kT/q$ is the thermal voltage. It can be observed that the conductivity increases exponentially with the applied voltage at stage II, whereas ∇E_{Fn} and ∇E_{Fp} change relatively slowly, and results in the variation in leakage current being dictated by the variation in conductivity of the regions along path I (note that in fact the path in the x direction of leakage current I_2 is mainly composed of path I) at stage II. Consequently, the leakage current varies exponentially with the voltage at stage II and the value of the ideality factor m in Equation (2) should be 2 according to Equation (10).

At stage III, the QFLS of the regions along path I is saturated, that is, E_{Fn}–E_{Fp} is a constant or varies particularly little. More specifically, saturation is reached when the QFLS in the TRs reaches about 0.8 eV, as shown in Figure 3f at stage III. In fact, most of the applied voltage drops on the bulk region at this time because of its finite resistivity, this is the same as when a diode is at a high-voltage level.[13] Therefore, the conductivity, ∇E_{Fn} and ∇E_{Fp} of the regions along path I all change notably slowly, leading to saturation of the leakage current.

4. Mechanism of Leakage Current Under Light Injection

Figure 4a–c shows the 3D band diagram and the corresponding 2D band diagram in the x direction at $y = 100$ μm and $y = 249.99$ μm at $U = 0$ V of the SCMS solar cell (Period = 4) under AM1.5G solar spectrum (correspond to Figure 3a,c,d).

The corresponding 2D band diagrams at other voltages are provided in Figure S4, Supporting Information. Unlike the dark condition, the quasi-Fermi levels are not flat under illumination at 0 V because of the diffusion current of light-generated carriers, which are generated everywhere over the whole solar cell (except TRs). Take particular notice of the inclined band in the TRs indicated by red dotted line, it means the leakage current appears after light injection (Equation (3) and (4)), which is driven by photogenerated voltage drop on both sides of each TR (the region consisting of HTL2, TR, and ETL1 is similar to a p–n junction). The light current density map by simulation of the complete structure when $U = 0$ V is shown in Figure S2d, Supporting Information. Figure 4d illustrates the schematic diagram of the leakage circuit under light and electric injection. Compared to electric injection only, there is an additional photoinduced leakage current I_{PL}. The I_{PL} is constant as long as the light intensity remains the same, no matter how much the electric injection is, this can be explained in terms of the same photogenerated voltage.

Figure 4e is a local detailed view of Figure 4c, consisting of HTL1/ETL1, HTL2/ETL2, and TR. The QFLS in the TR is 0.58 eV under AM1.5G solar spectrum, the corresponding I_{PL} is 3.7×10^{-7} A ($\approx$2.3 mA cm^{-2} for $L_{SCR} = 16.2$ mm), which can be read from Figure S1d, Supporting Information. Figure 4f can be obtained by subtracting I_{PL} from the light leakage current at different voltages. The remaining leakage current at stage I and stage II still exhibit good accordance with Equation (2) (and the light leakage current at stage III are almost the same as the dark leakage current as shown in Figure S3, Supporting Information), which is due to the fact that after subtracting the light injection only the electric injection remains. Therefore, the SCMS solar cells should satisfy the superposition principle as the conventional silicon solar cells, which means the current–voltage characteristic of an illuminated solar cell is the dark current–voltage characteristic shifted by the short-circuit photocurrent.[28] The fitting results are $R_{sh}' = 2.3 \times 10^6$ Ω, $I_{02}' = 1.8 \times 10^{-12}$ A, and $m' = 2$. Compared with the fitting results under only electric injection in Figure 2a, we recognize that only R_{sh} changes obviously, this is because photogenerated carriers cause the conductivity of the SCRs to increase. According to Equation (5), the injected photoconductivity in the SCRs is $\sigma_{pho} = 0.12$ S cm^{-1} when $\Delta N = 1 \times 10^{15}$ cm^{-3} and $\mu = 750$ cm^2 V s^{-1}.[29] And the original conductivity of the silicon wafer is $\sigma_o = 1/\rho = 0.001$ S cm^{-1}. Therefore, the resistance of path I under AM1.5G solar spectrum is as follows: $R_I' = \frac{1}{\sigma_o + \sigma_{pho}} \frac{L_1}{t \times d} = 8.26$ Ω cm $\times \frac{4200 \mu m}{250 \mu m \times 1 \mu m} = 1.39 \times 10^6$ Ω. R_{sh}' is larger than R_I' as there is no injected photoconductivity in the TRs due to shading. Additionally, the I_{PL} dominates at low-to-moderate voltages actually, since the QFLS in the TR is up to 0.58 eV under AM1.5G solar spectrum.

We can conclude that regardless of electric or light injection, it is the presence of voltage drop on both sides of each TR that cause leakage current, and the variation in the conductivity (resistance) of the regions along path I plays a decisive role in the variation in the leakage current under different injection. Furthermore, the effects of light injection and electric injection on the leakage current are independent of each other and can be superposed.
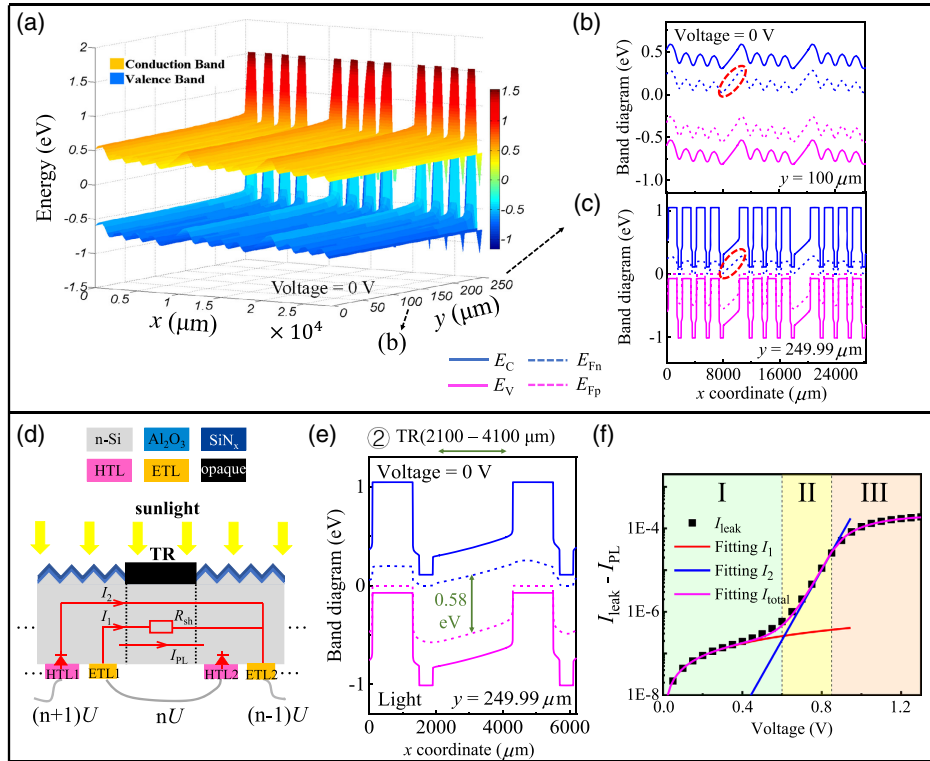
Figure 4. a) The 3D light band diagram and the corresponding 2D band diagram in the x direction at b) $y = 100\,\mu m$ and c) $y = 249.99\,\mu m$ of the SCMS solar cell (Period = 4) at $U = 0\,V$ (corresponds to Figure 3a–d). d) The schematic diagram of the leakage circuit under light and electric injection. e) A local detailed view of Figure c, consisting of HTL1/ETL1, HTL2/ETL2, and TR. ②: 2D band diagram in Figure 2c at $U = 0\,V$. f) (I_{leak}–I_{PL}) versus U curve of the SCMS solar cell (Period = 8) under AM1.5G solar spectrum. The fitting results are $R_{sh}' = 2.3 \times 10^{6}\,\Omega$, $I_{02}' = 1.8 \times 10^{-12}\,A$, and $m' = 2$.

5. Seven Methods to Suppress Leakage Current (Density) to Achieve the Homojunction SCMS Solar Cells with an Efficiency of ≥24.0%

Since the conductivity (resistance) of the regions along path I has a crucial effect on the variation in the leakage current, reducing the leakage current requires cutting down its conductivity (resistance). In this section, we use two paths in terms of resistance to reduce the leakage current (mainly change the resistance of each TR) and further improve the performance of the SCMS solar cells. According to the law of resistance, the resistance of each TR (R_{TR}) as a function of the voltage U can be described as

$$R_{TR}(U) = \rho(U)\frac{L}{td} = \frac{1}{d}\left(\frac{L}{t}\frac{1}{\sigma_o + \sigma_{inj}(U)}\right) \quad (11)$$

$\sigma_o = 1/\rho$ is the original conductivity of the TR, and $\sigma_{inj}(U)$ is the injected conductivity as a function of U. d is the length of TR in the z direction, but we do not take it into consideration here (this is a 2D simulation). As shown in **Figure 5**a, path A is to increase the original resistance of each TR (i.e., increasing ρ and L, and decreasing t); path B is to increase the recombination of carriers in the TRs, thereby attenuating the effect of carrier injection (light and electric injection) on conductivity of the TRs (i.e., reducing $\sigma_{inj}(U)$).

Figure 5b shows the dark $I_{leak} - U$ curves of the SCMS solar cell (Period = 8) at different ρ, which belong to path A to reduce the leakage current. The leakage current at stage I exhibits a significant decrease as ρ increases. At stage I, $\sigma_o \gg \sigma_{inj}(U)$, while at stage II, $\sigma_o \ll \sigma_{inj}(U)$. Therefore, increasing ρ (or decreasing σ_o) affects the leakage current only at stage I, exhibiting an increase of R_{sh}. The corresponding light (current density $\times N$)−(voltage/N) (J–V) curves and η at different ρ are presented in Figure 5c. Note that the horizontal axis in the figure is the total voltage/N, N is the number of sub-cells, and the J–V curves and η have taken the effect of shading on the surface of the TRs into account. We can observe that the SCMS solar cells require a silicon wafer with high ρ to be competitive. The η boosts from 6.8% at $\rho = 2\,\Omega\cdot cm$ to 18.2% at $\rho = 1000\,\Omega\,cm$. Short-circuit current density (J_{SC}), V_{OC}, and fill factor (FF) as a function of ρ can be found in Figure S5, Supporting Information.

Decreasing the wafer thickness t or increasing the length L of each TR, which belong to path A can also increase $R_{TR}(U)$ in the full voltage range according to Equation (11). But we have to pay attention to that the final efficiency of the SCMS solar cells results from the trade-off between the effect of various parameters on the leakage current and the effect on the SCRs. The detailed analysis of the effect of t and L on the final efficiency is provided in Figure S6, Supporting Information.

A high surface recombination rate in each TR (S_{TR}) or a low SRH lifetime in each TR (τ_{SRH}^{TR}) can effectively attenuate the
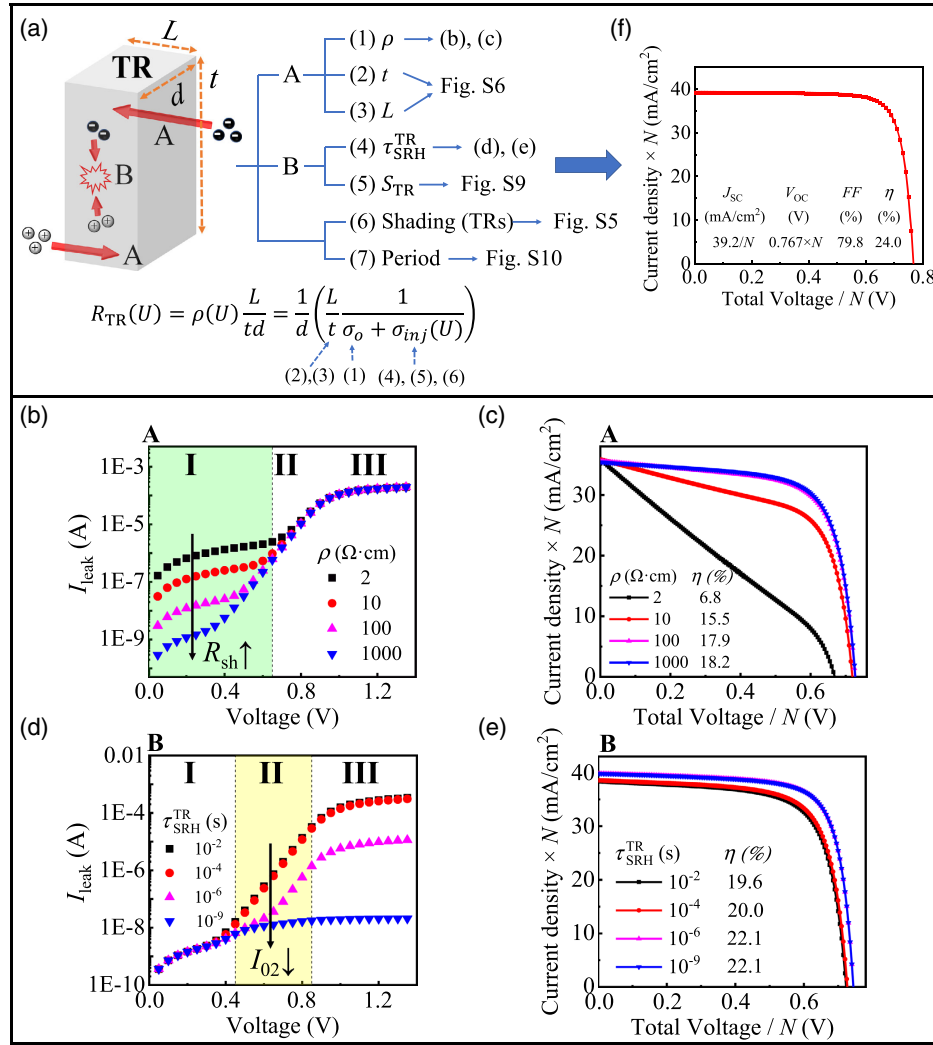
Figure 5. a) Schematic diagram of the physical process of carrier transport in the TR, illustrating paths A and B (5 methods in total) to reduce the leakage current. Methods (6) and (7) are also listed. b) Dark $I_{leak} - U$ curves and c) the corresponding light J–V curves of the SCMS solar cell (Period = 8) at different ρ, which belong to path A. Note that the horizontal axis in the figure is the total voltage/N, N is the number of sub-cells, and the J–V curves and η have taken the effect of shading on the surface of the TRs into account. d) Dark $I_{leak} - U$ curves and e) the corresponding light J–V curves of the SCMS solar cell (Period = 8, $L = 1000\,\mu m$) at different τ_{SRH}^{TR}, which belong to path B. f) Light J–V curve of the SCMS solar cell (Period = 14, $\rho = 1000\,\Omega\cdot cm$, $t = 62\,\mu m$, $L = 1000\,\mu m$, and $S_{TR} = 10^6\,cm\,s^{-1}$).

effect of carrier injection on conductivity of the TRs, which belong to path B. Here, only changing the SRH lifetime in each TR instead of that of the whole silicon wafer might not be industrially feasible or are just too expensive (such as using laser to execute a targeted damage to TR), the purpose of this is only to explain the physical mechanism. Figure 5d gives the dark $I_{leak} - U$ curves of the SCMS solar cell (Period = 8, $L = 1000\,\mu m$) at different τ_{SRH}^{TR}. A cliff-like drop in the leakage current at stage II and III can be observed as τ_{SRH}^{TR} decreases, exhibiting a sharp reduction of I_{02}, that is, $\sigma_{inj}(U)$ is reduced. When τ_{SRH}^{TR} is extremely small (i.e., recombination is extremely strong), such as $\tau_{SRH}^{TR} = 10^{-9}\,s$, $\sigma_{inj}(U) = 0$, only the stage I should exist as shown by the blue triangles in Figure 5d. This means that the injected conductivity can be eliminated, which is significant for the improvement of the efficiency of SCMS solar cell.

The corresponding light J–V curves and η are presented in Figure 5e. The η can still increases from 19.6% at $\tau_{SRH}^{TR} = 10^{-2}\,s$ to 22.1% at $\tau_{SRH}^{TR} = 10^{-9}\,s$ when other parameters are relatively optimized. However, the η saturates at $\tau_{SRH}^{TR} = 10^{-6}\,s$ although there is still an obvious drop in the I_{leak} from $\tau_{SRH}^{TR} = 10^{-6}\,s$ to $\tau_{SRH}^{TR} = 10^{-9}\,s$. Actually, the total loss current of the SCMS solar cells includes the leakage current flowing through each TR (I_{leak}) and the recombination current in each TR (I_{rec}). I_{rec} is similar to the recombination contribution caused by edge effect in silicon solar cells.[27,30] This is detailed in Figure S7, Supporting Information. Moreover, recombination exhibits a considerable benefit under illumination, which can significantly reduce injected photoconductivity and hence the I_{PL} as shown in Figure S7d, Supporting Information. J_{SC}, V_{OC}, FF, and η as a function of τ_{SRH}^{TR} are provided in Figure S8, Supporting

Information. S_{TR} works the same as τ_{SRH}^{TR}, the performance of SCMS solar cells at different S_{TR} are presented in Figure S9, Supporting Information. In a word, increasing recombination in the TRs has a significant effect on reducing the loss current. Obviously, the proposal of this unusual method requires a deep understanding of the leakage mechanism, and it has not been reported before.

It is worth mentioning that an outstanding improvement of the performance of SCMS solar cells as the Period increases can be observed in Figure S10, Supporting Information, η is optimized from 7.1% at Period = 2 ($L_{SCR} = 4.2$ mm) to 21.3% at Period = 14 ($L_{SCR} = 28.2$ mm). Dividing Equation (1) by the surface area S of a sub-cells in the SCMS solar cells gives

$$J = J_L - J_0 - \frac{I_{leak}}{S} \tag{12}$$

Increasing the Period (L_{SCR}) means increasing S, thereby the leakage current density I_{leak}/S is reduced, the performance of the SCMS solar cells can be remarkably improved in all aspects in spite of the unchanged leakage current. This indicates that the width of the sub-cells cannot be too small, otherwise η will be greatly compromised. In addition, shading the surface of the TRs is also a method to optimize the performance of SCMS solar cells as demonstrated in Figure S5, Supporting Information, this can be explained in terms of reducing light injection.

Utilizing the previous methods, that is, Period = 14, $\rho = 1000\ \Omega$ cm, $t = 62\ \mu m$, $L = 1000\ \mu m$, and $S_{TR} = 10^6$ cm s^{-1}, we can achieve the homojunction SCMS solar cell with a J_{SC} of $(39.2/N)$ mA cm^{-2}, a V_{OC} of $(0.767 \times N)$ V, a FF of 79.8%, and an η up to 24.0%. The corresponding light J–V curve is presented in Figure 5f. In fact, the efficiency can be even higher. In the previous sections, we have performed the simulation based on an infinite number of sub-cells connected in series. That is, there are N SCRs and $N - 1$ TRs and N tends to infinity. At this time, $N - 1/N$ is approximately equal to 1, that is, leakage exists on both left and right edges of each SCR. If only two sub-cells are connected in series, then $N - 1/N$ is equal to 0.5 and leakage only exists on one edge of each SCR. If the same parameters as aforementioned are used, we can obtain the SCMS solar cell with two sub-cells in series with a J_{SC} of $(40.6/N)$ mA cm^{-2}, a V_{OC} of $(0.772 \times N)$ V, a FF of 81.7%, and an η up to 25.6%. That is to say, the efficiency of the homojunction SCMS solar cells with the aforementioned parameters should be between 24.0% and 25.6%. The efficiency can be further improved by passivating contact technologies,[31] etc.

6. Conclusion

The study has been carried out by means of a TCAD-based numerical simulation based on an accurate simulation method. Our analysis revealed that the SCMS solar cells only have one more leakage channel, compared with normal IBC solar cells. We have extracted the leakage current and proposed and performed an in-depth analysis of an unconventional non-shunt resistance type of leakage mechanism under electric and light injection, which has not been reported before by investigating

the current density map, band diagram, and mathematical equation fitting of the leakage current, finding that the leakage current can be divided into three stages that are closely related to the variation in the conductivity (resistance) of the TRs under injection conditions. Then, based on our deep understanding of the leakage mechanism, several practical methods especially the unusual method of increasing the recombination to inhibit the rise in conductivity in the TR have been proposed to improve the efficiency of the SCMS solar cells by suppressing leakage current (density) at different stages, namely increasing ρ, L, S_{TR}, and Period, decreasing t and τ_{SRH}^{TR} and shading the surface of the TRs. Finally, the simulation exhibited that a V_{OC} of more than $(0.767 \times N)$ V (can reach $[0.772 \times N]$ V or even higher) and an η of more than 24.0% (can reach 25.6% or even higher) of the SCMS solar cells can be obtained. This confirms that the SCMS solar cells not only have the ability to output high voltage by controlling the number of sub-cells, but also have the potential to maintain high efficiency, which well meets the requirements of self-powered systems at low cost. After all, low cost is our permanent pursuit.

7. Methodology

7.1. Simulation Method

Since leakage existed at both the left and right edges of the SCRs as shown in Figure 1b,c, our simulation unit consisted of 2 half SCRs (i.e., only $P/2$ pairs of HTLs/ETLs inside the SCRs) and 1 TR, as a way to simulate the SCMS solar cells with Period = P, as shown in Figure S1a, Supporting Information. To easily understand the leakage mechanism, a homojunction SCMS solar cell was simulated here, that is, p^{++}–Si as HTL and n^{++}–Si as ETL, the simulation parameters can be found in **Table 1**. Shockley–Read–Hall (SRH) recombination, Auger recombination, Fermi–Dirac carrier statistics, and bandgap narrowing model were deployed into the simulation.[29] The default resistivity ρ and thickness t of silicon wafer were $\rho = 1000\ \Omega$ cm and $t = 250\ \mu m$, respectively, and the default length L of the TR in the x direction is $L = 2000\ \mu m$ in this paper. Additionally, this is a 2D (x and y) simulation, the length of the SCMS solar cell in the z direction is 1 μm by default. Note that all simulation

Table 1. Region parameters used in the simulation.

Region parameters[a]	n–Si	HTL (p^{++}–Si)	ETL (n^{++}–Si)
Doping concentration or Resistivity	2–1000 Ω cm	1×10^{21} cm^{-3}[b]	5×10^{20} cm^{-3}[b]
Layer thickness [μm]	30–250	1	1
Length [μm]	–	1200	400
SRH lifetime (τ_{SRH})[c] [ms]	10	10	10

[a]Other parameters: 1) The length of TR in the x direction is 50–4000 μm. 2) Gap between HTL and ETL is 200 μm. 3) SiN$_x$/Al$_2$O$_3$ is 65 and 15 nm, respectively. 4) The surface recombination rate at the p^{++}–Si/metal and n^{++}–Si/metal interface is 10^7 cm s^{-1} (thermal velocity limit). The rest can be found in ref.[29]; [b]Such high doping concentration is to suppress the high contact recombination at Si/metal interface[32]; [c]$1/\tau_{eff} = 1/\tau_{SRH} + 1/\tau_{Auger} + 1/\tau_{surf} + 1/\tau_{rad}$.[33]

results in this paper are based on the aforementioned simulation unit in Figure S1a, Supporting Information, except for the band diagram of three consecutive sub-cells in series in an SCMS solar cell (Period = 4) in Figure 3 and 4a–c and the performance of the SCMS solar cell with two sub-cells in series: $J_{SC} = (40.6/N)$ mA cm^{-2}, $V_{OC} = (0.772 \times N)$ V, $FF = 81.7\%$, and an $\eta = 25.6\%$, the simulation of the latter two were based on their complete structures.

7.2. Extraction Method of I$_{leak}$

I_{leak} was the sum of all current flowing through a cross section of the TR. It was assumed that the current density at any position was $J(x, y)$, and there was a cross section named S' at $x = x_0$ in the TR as demonstrated in Figure S1b, Supporting Information, then

$$I_{leak} = \int_{S'} J(x_0, y) dy \qquad (13)$$

It was noted that the current flowing through every cross section of the TR was equal no matter in the light condition or the dark condition since the TR was a field without sources. Additionally, we found that the leakage current exhibited an independence from Period revealed by Figure S1c,d, Supporting Information, which indicates that the leakage current only comes from the regions above HTL1/ETL1 and HTL2/ETL2. This also meant our developed simulation unit with $P/2$ pairs of HTL/ETL inside the SCR would not underestimate the leakage current as the leakage current did not come from all HTLs/ETLs, it could accurately simulate SCMS solar cells with Period = P.

7.3. Extraction Method of I$_{rec}$

It was assumed that the recombination rate at any position was $R(x, y)$, then

$$I_{rec} = q \iint_{TR} R(x, y) dx dy \qquad (14)$$

That is, I_{rec} is the area integral of the recombination rate in the TR as demonstrated in Figure S1b, Supporting Information.

Supporting Information

Supporting Information is available from the Wiley Online Library or from the author.

Acknowledgements

Conflict of Interest

The authors declare no conflict of interest.

Data Availability Statement

The data that support the findings of this study are available from the corresponding author upon reasonable request.

Keywords

[1] R. J. M. Vullers, R. van Schaijk, I. Doms, C. Van Hoof, R. Mertens, *Solid-State Electron.* **2009**, *53*, 684.

[2] Z. L. Wang, *Adv. Funct. Mater.* **2008**, *18*, 3553.

[3] Z. L. Wang, J. Chen, L. Lin, *Energy Environ. Sci.* **2015**, *8*, 2250.

[4] M. Kishi, H. Nemoto, T. Hamao, M. Yamamoto, S. Sudou, M. Mandai, S. Yamamoto, *presented at Eighteenth Inter. Conf. on Thermoelectrics*, IEEE, Maryland, USA **1999**.

[5] I. Stark, M. Stordeur, *presented at Eighteenth Inter. Conf. on Thermoelectrics*, IEEE, Maryland, USA **1999**.

[6] K. Itoigawa, H. Ueno, M. Shiozaki, T. Toriyama, S. Sugiyama, *J. Micromech. Microeng.* **2005**, *15*, S233.

[7] T. Ungan, L. M. Reindl, *presented at 25th IEEE Instrumentation and Measurement Technology Conf.*, IEEE, Victoria, Canada **2008**.

[8] R. Vullers, H. Visser, B. O. Het Veld, V. Pop, *presented at 2nd Symp. on Micro Environmental Machine Systems*, Sendai, Japan **2008**.

[9] E. Kabir, P. Kumar, S. Kumar, A. A. Adelodun, K.-H. Kim, *Renewable Sustainable Energy Rev.* **2018**, *82*, 894.

[10] J. Zhao, J. Zha, Z. Zeng, C. Tan, *J. Mater. Chem. A.* **2021**, *9*, 18887.

[11] M. J. Kumar, M. Maheedhar, P. P. Varma, *IEEE Trans. Electron Devices* **2015**, *62*, 4345.

[12] A. Savio, S. Monfray, C. Charbuillet, T. Skotnicki, *IEEE Trans. Electron Devices* **2009**, *56*, 1110.

[13] S. M. Sze, K. K. Ng, *Physics of Semiconductor Devices*, John Wiley&Sons, Hoboken, NJ **1981**.

[14] J. Johansson, *Master Thesis*, Lunds University (Sweden), **2007**.

[15] M. Yamaguchi, K.-H. Lee, K. Araki, N. Kojima, *J. Phys. D: Appl. Phys.* **2018**, *51*, 133002.

[16] J.-L. Hou, C.-H. Wu, T.-J. Hsueh, *Sens. Actuators, B* **2014**, *197*, 137.

[17] T. D. Lee, A. U. Ebong, *Renewable Sustainable Energy Rev.* **2017**, *70*, 1286.

[18] F. Urbain, V. Smirnov, J. P. Becker, A. Lambertz, F. Yang, J. Ziegler, B. Kaiser, W. Jaegermann, U. Rau, F. Finger, *Energy Environ. Sci.* **2016**, *9*, 145.

[19] A. Al-Ashouri, E. Khnen, B. Li, A. Magomedov, S. Albrecht, *Science* **2020**, *370*, 1300.

[20] A. Richter, R. Müller, J. Benick, F. Feldmann, B. Steinhauser, C. Reichel, A. Fell, M. Bivour, M. Hermle, S. W. Glunz, *Nat. Energy.* **2021**, *6*, 429.

[21] A. Jäger-Waldau, PV Status Report 2019, https://doi.org/10.2760/326629 (accessed: October 2021).

[22] M. Arif, M. Rahman, W. Y. San, *Int. J. Adv. Manuf. Technol.* **2012**, *63*, 481.

[23] S. Nordmann, B. Berghoff, A. Hessel, N. Wilck, B. Osullivan, M. Debucquoy, J. John, S. Starschich, J. Knoch, *Renewable Energy* **2016**, *94*, 90.

[24] S. Nordmann, B. Berghoff, A. Hessel, B. Zielinsk, J. John, S. Starschich, J. Knoch, *Sol. Energy Mater. Sol. Cells* **2019**, *191*, 422.

[25] M. D. Lammert, R. J. Schwartz, *IEEE Trans. Electron Devices* **1977**, *24*, 337.

[26] K. Yoshikawa, H. Kawasaki, W. Yoshida, T. Irie, K. Konishi, K. Nakano, T. Uto, D. Adachi, M. Kanematsu, H. Uzu, K. Yamamoto, *Nat. Energy.* **2017**, *2*, 1.

[27] K. R. Mcintosh, *PhD Thesis*, University of New South Wales (Sydney, Australia), **2001**.

[28] F. A. Lindholm, J. G. Fossum, E. L. Burgess, *IEEE Trans. Electron Devices* **1979**, *26*, 165.

[29] Silvaco, Atlas user manual 2019, https://www.silvaco.com/, (accessed: August 2021).

[30] H. Lin, J. Wang, Z. Wang, Z. Xu, P. Gao, W. Shen, *Nano Energy.* **2020**, *74*, 104893.

[31] T. G. Allen, J. Bullock, X. Yang, A. Javey, S. De Wolf, *Nat. Energy.* **2019**, *4*, 914.

[32] J. Zhao, A. Wang, P. Altermatt, M. A. Green, *Appl. Phys. Lett.* **1995**, *66*, 3636.

[33] M. J. Kerr, A. Cuevas, *J. Appl. Phys.* **2002**, *91*, 2473.